Check for updates

Green and efficient synthesis of 5-amino-1*H*-pyrazole-5-carbonitriles utilizing novel modified LDH†

Sarieh Momeni and Ramin Ghorbani-Vaghei [ID] *

This research introduced a novel nano catalyst, LDH@PTRMS@DCMBA@CuI, developed from nano copper immobilized on a layered double hydroxide modified with a new type of sulfonamide: N_1,N_3-dicarbamimidoylbenzene-1,3-disulfonamide (DCMBA). This catalyst demonstrated significant activity and selectivity in synthesizing 5-amino-1*H*-pyrazole-5-carbonitrile derivatives. The derivatives were produced *via* a three-component one-pot reaction combining benzaldehydes, malononitrile, and phenyl hydrazine in H_2O/EtOH solvent at 55 °C. This innovative synthesis strategy offered several advantages, including eco-friendliness, simplicity, stability, mild reaction conditions, easy purification of products, short reaction times (15–27 min), and excellent yields (85–93%). Additionally, the green methodology was validated by the catalyst's reusability over four consecutive cycles without significant loss of catalytic activity.

1. Introduction

Layered double hydroxides (LDHs) are attracting considerable interest because of their applications across various fields such as catalyst precursors, anion exchangers, absorbents, and bioactive materials. Important factors in LDH synthesis include the extent of cation substitution from M^{2+} to M^{3+}, the specific types of cations and interlayer anions, as well as the pH, temperature, and environmental conditions during preparation.[1–3] Various synthetic methods exist for preparing LDHs, including regeneration, ion exchange, hydrothermal synthesis, and co-precipitation, with the last being the most effective. The co-precipitation method is advantageous because it enables the direct incorporation of various anionic species into LDHs that are challenging to achieve using other methods. Zn–Cr-LDHs formed from inorganic anions such as Cl^-, NO_3^-, CO_3^{2-}, and SO_4^{2-} were successfully synthesized using co-precipitation and anion exchange methods.[4–7]

The field of green chemistry is proposing innovative approaches with a strong emphasis on environmental sustainability. Chemists are increasingly adopting green techniques, such as using green solvents like water, conducting solvent-free syntheses, employing cost-effective catalysts, and implementing one-pot multicomponent reactions.[8–11] The development of multicomponent reactions (MCRs) is a highly attractive research area because they enable the formation of products in a single step, and a wide variety of products can be obtained simply by altering the reaction components. These reactions are particularly advantageous due to their high yields, short reaction times, and the principles of atom economy.[12] Additionally, MCRs significantly reduce the use of solvents and energy, making them a more sustainable and efficient approach in chemical synthesis. These benefits make MCRs a valuable protocol in the pursuit of greener and more cost-effective chemical processes.[13–15]

Pyrazole, characterized by its five-membered ring structure with two nitrogen atoms, has emerged as an important member within the wide array of heterocyclic compounds, distinguishing itself as a notable class of N-heterocycles.[16] Pyrazoles exhibit a wide array of pharmaceutical and biological activities, making them highly valuable in medical research and drug development. These compounds are known for their antimalarial,[17] antibacterial,[18] antioxidant,[19] antiparasitic,[20] anti-viral activities,[21] antidepressant,[22] anticancer,[23] and anti-inflammatory[24] properties. Their unique biological activity has led to extensive studies and applications in developing new therapeutic agents, underscoring the importance of pyrazoles in medicinal chemistry.

Several successful drugs have been derived from the pyrazole structure, including Celebrex (R) and Viagra (R), which are known inhibitors of PDE-5,[25,26] Zoniporide, an inhibitor of the sodium hydrogen ion exchanger, and PNU-32945, which inhibits HIV reverse transcriptase.[27,28] These drugs showcase the versatility and therapeutic potential of the pyrazole in pharmaceutical development. To synthesize 5-amino-1*H*-pyrazole-4-carbonitrile, various catalysts have been utilized, such as sodium ascorbate,[29] $[HMIM]C(NO_2)_3$,[30] DABCO,[31] CPS-CDMNPs,[32] Fe_3O_4@Alg@CPTMS@Arg,[33] palladium and copper,[34] ionic liquids,[35] and Glu@Fe_3O_4.[36] These catalysts enable efficient multicomponent synthesis of pyrazole derivatives. The development and utilization of new catalysts

Department of Organic Chemistry, Faculty of Chemistry and Petroleum Sciences, Bu-Ali Sina University, Hamedan, Iran. E-mail: rgvaghei@yahoo.com; ghorbani@basu.ac.ir

† Electronic supplementary information (ESI) available. See DOI: https://doi.org/10.1039/d4na00577e

underscore the ongoing progress in chemical synthesis, which is focused on producing effective pharmaceutical compounds. These advancements enable more efficient and selective reactions, leading to the creation of drugs with improved efficacy and reduced side effects. By innovating catalyst design and application, chemists can streamline synthetic pathways, enhance yields, and minimize environmental impact, ultimately contributing to the discovery and production of next-generation therapeutics.

In this study, a novel catalyst was designed and synthesized, consisting of nano copper stabilized on layered double hydroxide functionalized with the ligand N_1,N_3-dicarbamimidylbenzene-1,3-disulfonamide (DCMBA). Then, a three-component, one-pot synthesis method for pyrazolyl-5-amino-pyrazole-4-carbonitrile derivatives is presented by reacting malononitrile, phenyl hydrazine and various benzaldehyde derivatives in the presence of this catalyst within a water/ethanol solvent at 55 °C. Remarkably, these derivatives are synthesized with high yield and in minimal reaction time.

2. Experimental

2.1. The synthesis of LDHs

Zn–Cr-LDH was synthesized according to an established procedure, briefly summarized as follows. Chromium nitrate $(Cr(NO_3)_3 \cdot 9H_2O)$ and zinc nitrate $(Zn(NO_3)_2 \cdot 6H_2O)$ were combined in a 2 : 1 molar ratio and dissolved in deionized water. The solution was stirred vigorously while the pH was adjusted to 11.5 with 2 M NaOH aqueous solution. The mixture was then kept at a constant temperature for 18 h. The resulting green precipitate was filtered, washed with distilled water, and dried in an oven at 60 °C for 24 h.[37]

2.2. Preparation of LDHs coated with 3-chloropropyltrimethoxysilane (LDHs@PTRMS)

For the activation of LDH, 3-chloropropyltrimethoxysilane was utilized. The process began with dissolving 1 g of the previously synthesized LDH in 50 mL of toluene. Following this, 2 mL of 3-chloropropyltrimethoxysilane was introduced to the solution. The mixture was then subjected to refluxing with constant stirring for 24 h to ensure thorough interaction between the LDH and the silane compound. After the reflux period, the resulting precipitate was collected using filter paper. This precipitate was washed three times with toluene and once with ethanol to remove any unreacted materials and impurities. Finally, the cleaned precipitate was dried in an oven at 60 °C to obtain the activated LDH.

2.3. Preparation of 1,3-benzenedisulfonyl chloride (as the precursor of the N_1,N_3-dicarbamimidoylbenzene-1,3-disulfonamide ligand)

To begin, 16.5 mmol of PCl₅ was added as the chlorination agent to a container holding 5.00 g (18 mmol) of 1,3-benzene-disulfonic acid disodium salt. The mixture was then sterilized and heated to 65 °C, allowing the reaction to proceed for 2 h. Once the reaction was complete, 100 g of dry ice was carefully added to the mixture. Following this, 100 mL of chloroform was introduced into the reaction vessel. The mixture was then thoroughly stirred to ensure proper mixing, and the organic layer was separated from the aqueous phase with a decanter funnel.

2.4. Ligand synthesis: N_1,N_3-dicarbamimidoylbenzene-1,3-disulfonamide (DCMBA)

In a 50 mL flask, 6 mmol of guanidine was dissolved in 10 mL of methanol. Gradually, 3 mmol of 1,3-benzenedisulfonyl chloride was added to the solution, and the reaction mixture was then refluxed with vigorous stirring for 20 h. After the reaction was complete, the mixture was collected by centrifugation, washed three times with methanol and once with acetonitrile, and then dried in an oven at 60 °C.

2.5. Synthesis of LDH capped with N_1,N_3-dicarbamimidoylbenzene-1,3-disulfonamide ligand (LDH@PTRMS@DCMBA)

In a 250 mL flask, 0.3 g of LDH activated with 3-chloropropyl-trimethoxysilane (prepared in previous steps) was dispersed in 50 mL of toluene using an ultrasonic device for 15 min. Then, 0.5 g of the ligand N_1,N_3-dicarbamimidoylbenzene-1,3-disulfonamide was added, and the reaction mixture was subjected to reflux with a magnetic stirrer for 48 h. After the reaction was complete, the precipitate was collected by centrifugation and washed three times with toluene, once with ethanol, and once with methanol, and dried in an oven at 60 °C for 24 h.

2.6. Catalyst synthesis: copper iodide immobilized on LDH coated with DCMBA ligand (LDH@PTRMS@DCMBA@CuI)

Copper iodide was synthesized following previous work.[38] To load copper nanoparticles, 0.5 g of the LDH@PTRMS coated with DCMBA was dispersed in 20 mL of ethanol using ultra-sonication for 5 min. Then, 0.3 g of copper nanoparticles was added to the mixture, which was subjected to reflux conditions for 24 h. After the formation of nano copper stabilized on the coated layered double hydroxides, the nanoparticles were collected by centrifugation, washed three times with 10 mL of ethanol, and dried under vacuum at 60 °C for 24 h. Scheme 1 illustrates the steps involved in catalyst synthesis.

2.7. General method for the synthesis of 5-amino-1,3-diphenyl-1H-pyrazole-4-carbonitrile derivatives in the presence of LDH@PTRMS@DCMBA@CuI nanoparticles

In a test tube containing phenyl hydrazine (1 mmol), benzaldehyde derivatives (1 mmol), malononitrile (1 mmol), and the LDH@PTRMS@DCMBA@CuI catalyst (0.05 g), the mixture was stirred in H_2O/EtOH solvent (0.5 : 0.5 mL) at 55 °C using a magnetic stirrer for an appropriate period of time. The advancement of the reaction was tracked using TLC (n-hexane/ethyl acetate: 5 : 5 mL) to observe the transformation of reactants into products. Once the reaction reached completion and the desired compound was obtained, the mixture was allowed to cool
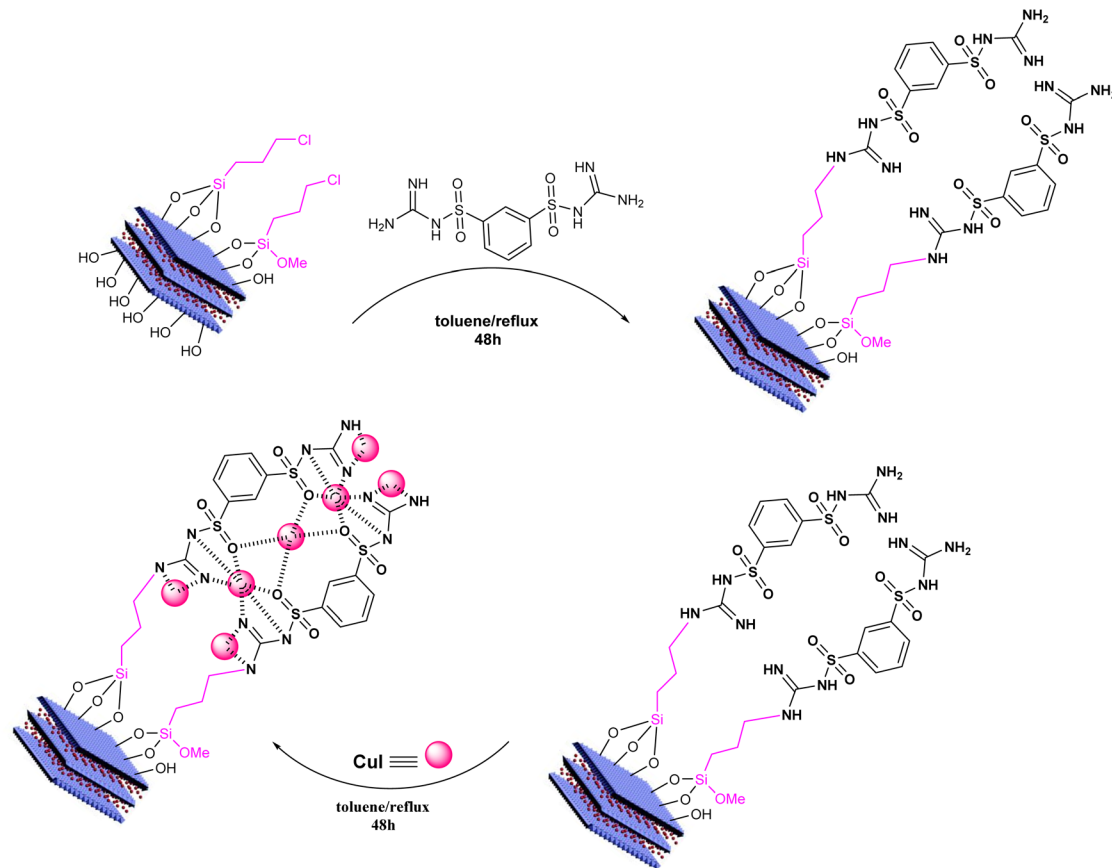
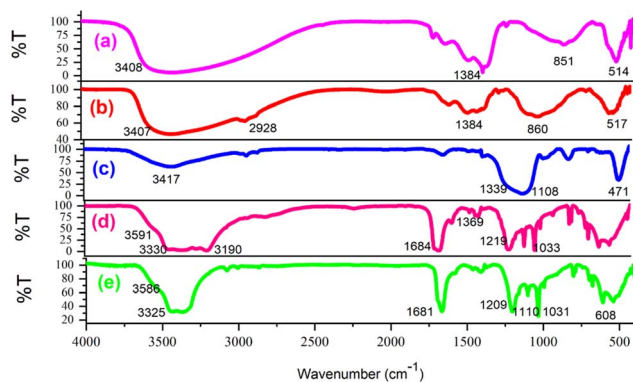**Scheme 1** Synthesis steps of the LDH@PTRMS@DCMBA@CuI catalyst.

Fig. 1 FTIR spectra of (a) LDH, (b) LDH@PTRMS, (c) the DCMBA ligand, (d) LDH@PTRMS@DCMBA and (e) LDH@PTRMS@DCMBA@CuI.

to room temperature. To isolate the catalyst, 3 mL of either hot ethanol or chloroform was introduced into the reaction mixture. Subsequently, the catalyst (LDH@PTRMS@DCMBA@CuI) was separated through centrifugation, washed with ethanol, and subsequently dried in an oven at 60 °C to remove any residual solvent and moisture. The solvent of the reaction mixture was evaporated, and the products were recrystallized with ethanol, yielding the compounds with high yield. The products were identified using FTIR, ^{1}H NMR, and ^{13}C NMR spectra, and the melting points of all products were recorded.

3. Results and discussion

3.1. Investigating the spectroscopic pattern of catalyst synthesis: nano copper immobilized on the layered double hydroxides coated with the N_1,N_3-dicarbamimidoylbenzene-1,3-disulfonamide ligand

Following the synthesis of the catalyst, various analyses were conducted to confirm and characterize the LDH@PTRMS@ DCMBA@CuI catalyst. These analyses included Fourier-transform infrared spectroscopy (FT-IR), elemental mapping, energy-dispersive X-ray spectroscopy (EDX), X-ray diffraction (XRD), field emission scanning electron microscopy (FESEM), and thermal analysis (DSC and TGA).

Fig. 1 presents the FT-IR spectrum for various samples: (a) the layered double hydroxide, (b) LDH@PTRMS, (c) the DCMBA ligand, (d) LDH@PTRMS@DCMBA, and (e) LDH@PTRMS@NDBD@CuI. Section (a) shows the spectrum for LDH, with peaks ranging from 2500 to 3490 cm^{-1} attributed to the hydroxides present on LDH, and peaks within 1380–1400 cm^{-1} indicating the stretching vibrations of the interlayer nitrate anion. Additionally, the peak at 814 cm^{-1} corresponds to metal–oxygen stretching vibrations. Section (b): in addition to all the peaks observed in the previous stage, the 2928 cm^{-1} peak represents LDH functionalized with 3-chloropropyltrimethoxysilane, which signifies C–H stretching
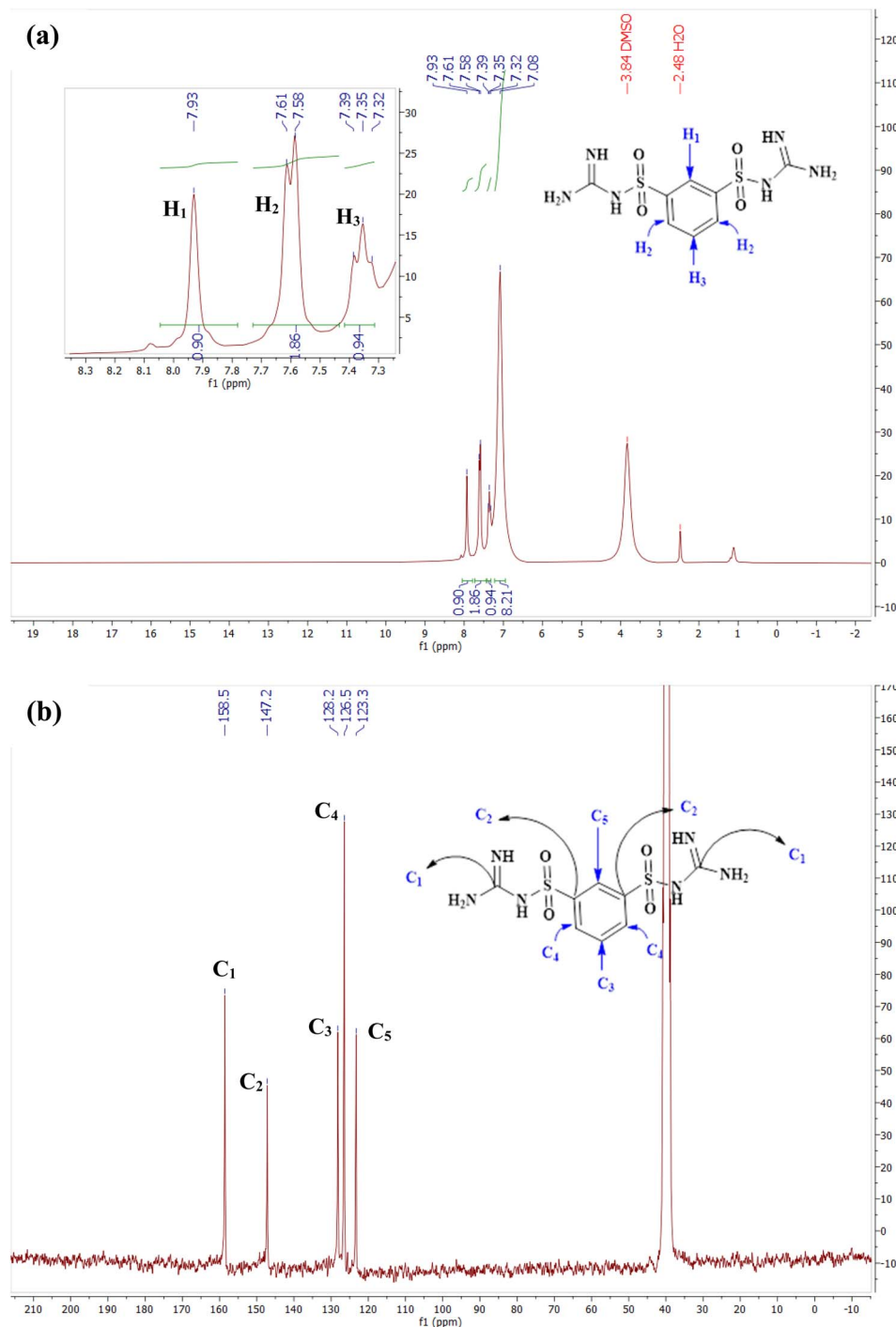
Fig. 2 (a) ^{1}H NMR and (b) ^{13}C NMR spectra of the DCMBA ligand in DMSO-d_6 solvent.

vibrations.[38] Part (c) details the synthesis of the DCMBA ligand, where a broad absorption peak between 1108 and 1339 cm^{-1} corresponds to the stretching vibrations of S=O, and an absorption peak around 3417 cm^{-1} corresponds to the stretching vibrations of the NH group. Part (d) describes the attachment of the ligand to the surface of the layered double hydroxide activated with 3-chlorotrimethoxysilane. Here, the stretching vibrations of the NH group are observed between 3190 and 3330 cm^{-1}, the stretching vibrations of the hydroxyl

group of LDH appear at 3591 cm^{-1}, and the peaks at 1100 cm^{-1} and 1369 cm^{-1} correspond to the S=O stretching vibrations of the ligand. Part (e) pertains to the deposition of nano copper on the catalyst surface, where the intensity of the stretching vibrations of NH and S=O groups decreases, indicating their interaction with the nanomaterials.

Fig. 2 displays the ^{1}H NMR and ^{13}C NMR spectra of the DCMBA ligand in DMSO-d_6 solvent. Part (a) focuses on the ^{1}H NMR spectrum. The singlet peak at 7.93 δ, with an integral of 1,
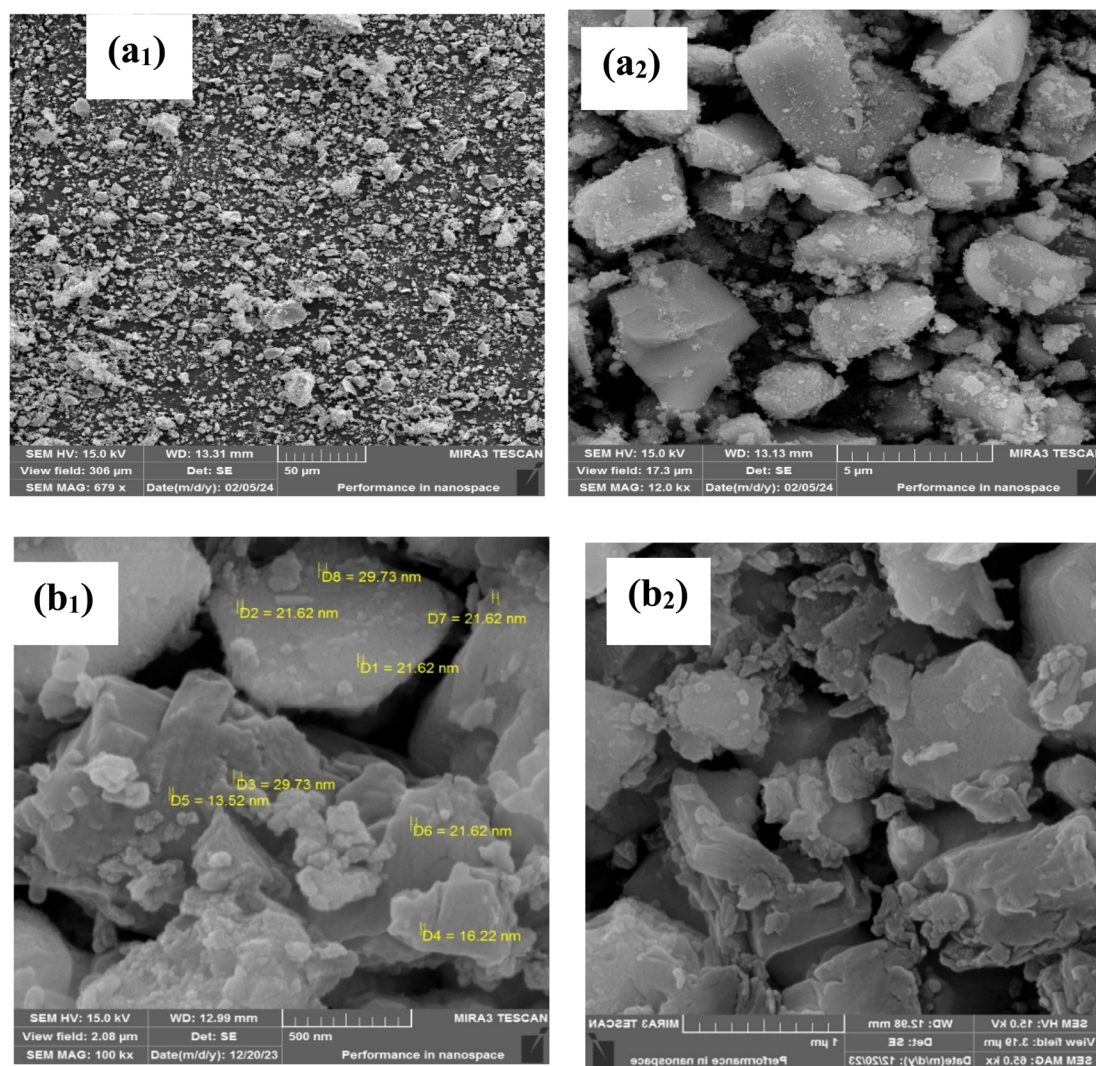
Fig. 3 FESEM images of (a_1 and a_2) LDH@PTRMS and (b_1 and b_2) LDH@PTRMS@DCMBA@CuI catalyst.

corresponds to a proton on the benzene ring (H_1). The doublet peak between 7.61 and 7.51 δ, with an integral of 2, is associated with two benzene protons (H_2). The triplet peak at 7.32–7.39 δ, with an integral of 1, is also attributed to a benzene proton (H_3). The NH protons related to guanidine bound to SO_2 appear as a broad peak centered at 7.08 δ, with an integral of 8.

Part (b) presents the ^{13}C NMR spectrum of the DCMBA ligand. The peak at 158.5 δ corresponds to the two carbons attached to the amines (C_1). The peak at 147.2 δ is related to the two benzene carbons connected to the SO_2 group (C_2). The peak at 128.2 δ corresponds to another carbon on the benzene ring (C_3), and the peak at 126.5 δ is attributed to two more benzene carbons (C_4). The final benzene carbon appears at 123.3 δ (C_5).

To gain further insight into the morphology and size of the synthesized LDH@PTRMS@DCMBA@CuI nanoparticles, FESEM analysis was conducted. Fig. 3 reveals that the LDH particles exhibit a stacked sheet-like structure with sizes ranging from approximately 1 to 4 μm, indicating that the catalyst forms as sheets (a_1 and a_2). The copper nanoparticles,

depicted in the image, appear to be nearly spherical and are anchored to the LDH surface, with sizes ranging from about 16 to 29 nm (b_1 and b_2).

TGA and DSC analyses were employed to assess the thermal stability of the LDH@PTRMS@DCMBA@CuI catalyst (Fig. 4). The TGA analysis indicated several stages of mass reduction as the temperature increased. The initial slight mass loss (about 3%) below 200 °C is attributed to the evaporation of water and organic solvents in the layers. A more significant weight loss (about 13%) around 370 °C corresponds to the decomposition of organic groups, confirming that the LDH@PTRMS@DCMBA@CuI catalyst remains stable up to 350 °C. Additionally, the DSC curves demonstrated that the LDH nano catalyst maintains its stability at temperatures below 350 °C.

The XRD analysis was utilized to investigate the crystallinity and particle size of the catalyst. In Fig. 5, the XRD patterns illustrating various stages of catalyst synthesis are depicted: (a) LDH, (b) LDH@PTRMS,[37] and (c) LDH@PTRMS@DCMBA@CuI. In part (a), the peaks observed at 11.2°, 24°, 34°, 35°, 37°,
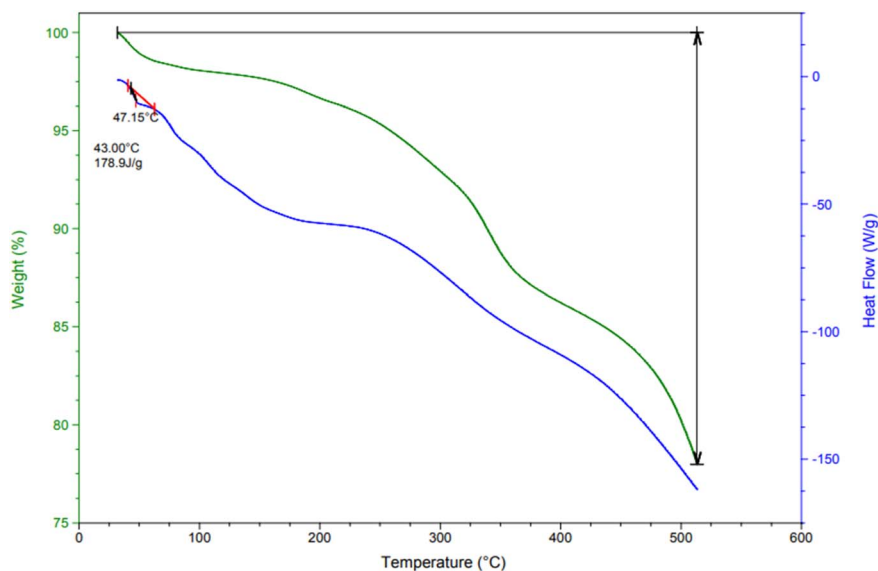
Fig. 4 TGA and DSC thermal analyses of the LDH@PTRMS@DCMBA@CuI catalyst.
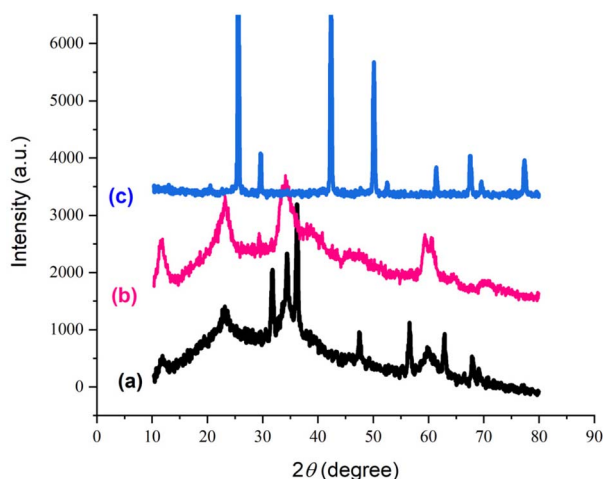

Fig. 5 X-ray diffraction of the catalyst and its intermediates, (a) layered double hydroxide, (b) LDH@PTRMS, and (c) LDH@PTRMS@DCMBA@CuI.

48°, 58°, 59°, and 68° correspond to the crystal planes (003), (006), (101), (012), (015), (018), (108), (110), and (113), respectively, indicating the Zn/Cr-LDH structure. In part (b), after activating the LDH surface with 3-chlorotrimethoxysilane, the same peaks are present, but with varying intensities. In part (c), the presence of peaks at 10°, 20°, 25°, 40°, 50°, 60°, 70°, and 80° signifies the high crystallinity and extensive structural regularity exhibited by these samples. Additionally, these patterns confirm that copper nanoparticles are effectively immobilized on the LDH@PTRMS@DCMBA@CuI structure.

The EDX analysis provided insight into the chemical properties and elemental composition of the synthesized catalyst, affirming the presence of chromium, zinc, nitrogen, carbon, oxygen, copper, and iodine atoms within the catalyst construction (Fig. 6). Furthermore, the elemental composition analysis of the synthesized catalyst verified the presence of all mentioned elements and revealed a homogeneous distribution of these elements throughout the composition (Fig. 7).

3.2. Catalytic application of the LDH@PTRMS@DCMBA@CuI in the preparation of 5-amino-1,3-diphenyl-1*H*-pyrazole-4-carbonitrile derivatives

After validating the novel LDH@PTRMS@DCMBA@CuI nano catalyst, the synthesis of 5-amino-1,3-diphenyl-1*H*-pyrazole-4-carbonitrile derivatives was undertaken to assess its catalytic efficacy. Initially, in a preliminary investigation to determine optimal conditions, malononitrile (1 mmol), phenyl hydrazine (1 mmol), and 4-chloro-benzaldehyde (1 mmol) were chosen as model substrates. The model reaction was conducted employing various solvents, such as water, ethanol, water/ethanol, methanol, and acetonitrile, as well as under solvent-free conditions, at varying temperatures, and with different amounts of catalyst. As shown in Table 1, the absence of the LDH@PTRMS@DCMBA@CuI nano catalyst resulted in longer reaction times, higher required temperatures, and reduced yield. A wide range of temperatures, from room temperature to 100 °C, was explored. The results demonstrated that the choice of solvent has a significant impact on product yield. Ethanol and methanol both increased the reaction yield compared to other solvents, with the highest yield achieved using a water/ethanol solvent mixture, The highest yield (93%) and the shortest reaction time (15 min) were achieved using 0.05 g of the LDH@PTRMS@DCMBA@CuI catalyst at 55 °C in a water/ethanol solvent mixture. The results are summarized in Table 1.

Table 2 compares the catalytic activity of LDH@PTRMS@DCMBA@CuI with its related intermediates in the model reaction involving phenyl hydrazine (1 mmol), malononitrile (1 mmol), and 4-chlorobenzaldehyde (1 mmol). As shown in the table, using LDH in the reaction resulted in a low yield (23%). Upon activation of LDH with PTRMS, the
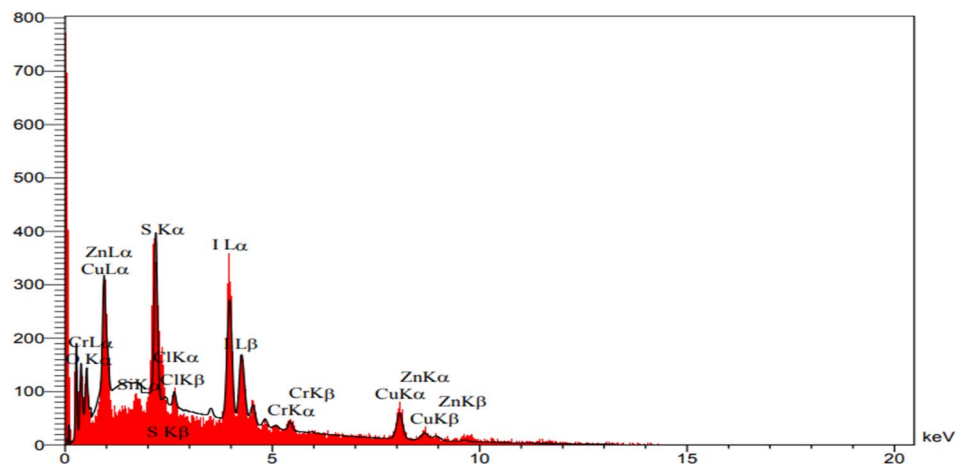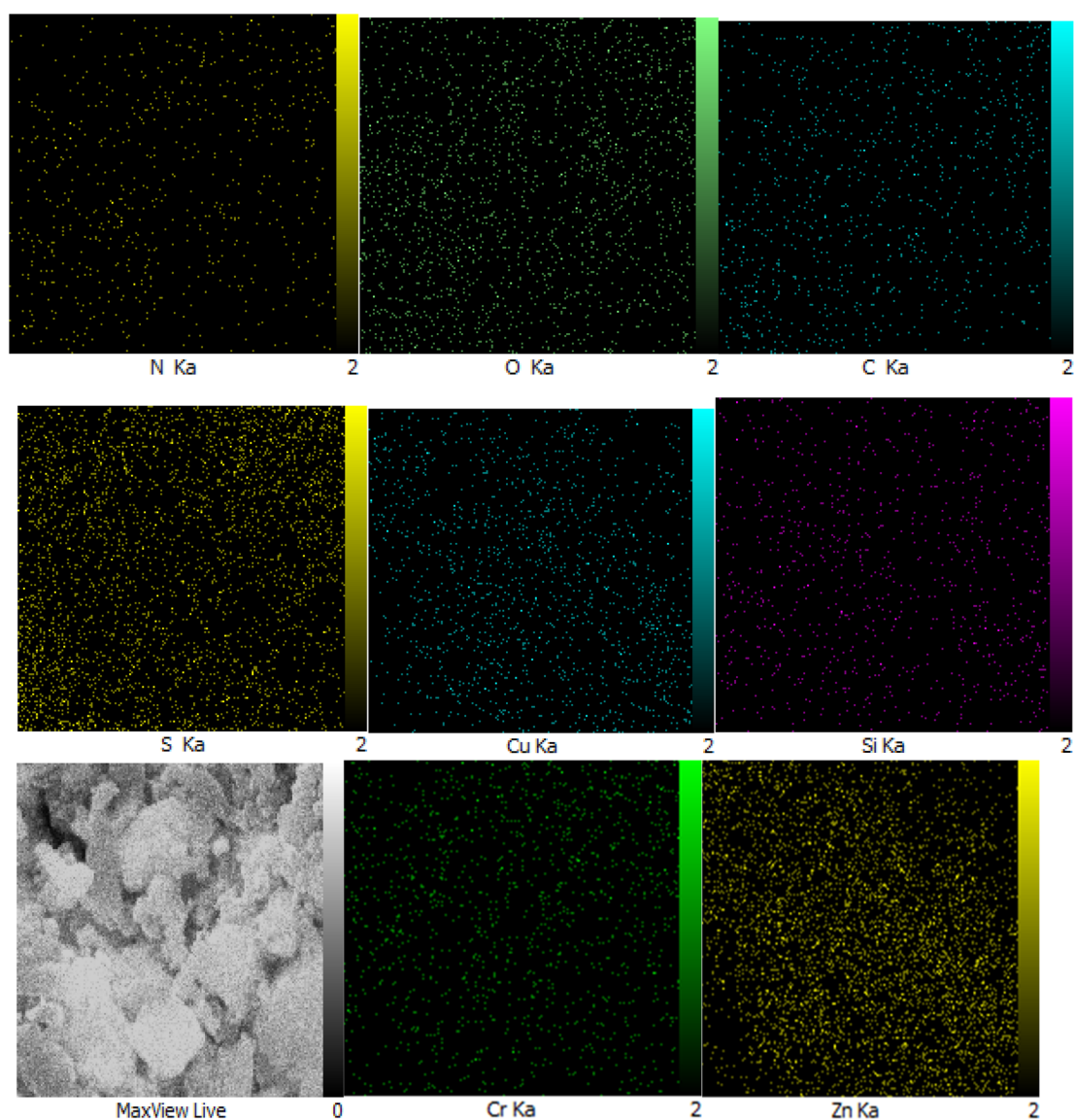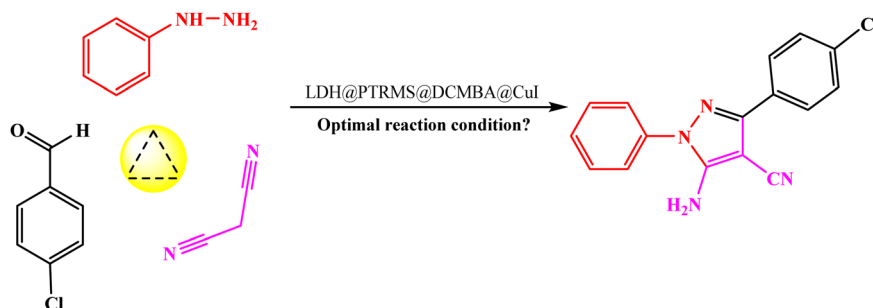
Fig. 6 EDX analysis of the LDH@PTRMS@DCMBA@CuI catalyst.

Fig. 7 Elemental mapping analysis (MAPPING) of the LDH@PTRMS@DCMBA@CuI catalyst.

© 2024 The Author(s). Published by the Royal Society of Chemistry

Table 1 Optimization of reaction conditions for the synthesis of 5-amino-3-(4-chlorophenyl)-1-phenyl-1H-pyrazole-4-carbonitrile

Entry	Solvent	Load of catalyst (mg)	Temperature (°C)	Time (min)	Yield (%)
1	—	—	100	60	Trace
2	—	50	70	20	83
3	EtOH	50	Reflux	40	42
4	H_2O	50	Reflux	50	Trace
5	$EtOH : H_2O$	50	Reflux	15	93
6	MeOH	50	Reflux	50	35
7	EtOAc	50	Reflux	55	Trace
8	CH_3CN	50	Reflux	45	Trace
9	$EtOH/H_2O$ (1 : 1)	50	70	12	93
10	$EtOH/H_2O$ (1 : 1)	50	60	15	93
11	$EtOH/H_2O$ (1 : 1)	15	55	50	45
12	$EtOH/H_2O$ (1 : 1)	25	55	45	56
13	$EtOH/H_2O$ (1 : 1)	35	55	30	80
14	**$EtOH/H_2O$ (1 : 1)**	**50**	**55**	**15**	**93**
15	$EtOH/H_2O$ (1 : 1)	50	r.t	30	65

Table 2 Comparison of the catalytic activity of LDH@PTRMS@DCMBA@CuI, its related intermediates and two other heterogeneous catalysts by performing the model reaction

Entry	Catalyst	Time	Yield (%)
1	LDH	60	23
2	LDH@PTRMS	60	30
3	LDH@PTRMS@DCMBA	45	50
4	LDH@TRMS@DCMBA@CuI	15	93
5	LDH@TRMS@BDSA@Ni[39]	30	Trace
6	LDH@TRMS@NDBD@Cu(NO$_3$)$_2$ (ref. 37)	30	Trace

product yield increased slightly to 30%, with the reaction time remaining at 60 minutes. However, functionalizing the surface with the DCMBA ligand significantly improved the yield to 50% and reduced the reaction time to 45 minutes. By stabilizing nano copper iodide on the surface of LDH functionalized with the DCMBA ligand, the reaction efficiency significantly increased to 93%, and the reaction time was reduced to just 15 minutes, demonstrating the catalyst's high efficiency. Also, the reaction of the model was investigated in the presence of two catalysts LDH@TRMS@BDSA@Ni[39] and LDH@TRMS@NDBD@Cu(NO$_3$)$_2$,[37] the results showed that an insignificant product was obtained in the presence of these catalysts.

Subsequently, the optimal reaction conditions were applied to synthesize various other 5-amino-1,3-diphenyl-1H-pyrazole-4-carbonitrile derivatives using different aryl aldehydes with electron-donating or electron-withdrawing groups (Table 3). The results, as summarized in Table 3, demonstrate that all derivatives were readily synthesized with high yields, underscoring the remarkable catalytic activity of the LDH@PTRMS@DCMBA@CuI nano catalyst in the synthesis of 5-amino-1,3-diphenyl-1H-pyrazole-4-carbonitrile derivatives.

The Hammett equation, a linear free energy relationship, clarifies how reaction energetics are influenced by substituent effects. Changes in the reaction's free energy impact the activation energy of the transition state. By plotting the logarithm of the rate constant ratio ($\log(k_X/k_H)$) against the substituent constant (σ) for various groups positioned meta and para to the reaction center, as shown in Fig. 8 of the Hammett diagram, distinct patterns emerge. Notably, the positive slope in the Hammett plot indicates that electron-withdrawing groups accelerate the reaction rate, although the effect is minimal due to the low slope value.

The proposed mechanism for synthesizing 5-amino-1,3-diphenyl-1H-pyrazole-4-carbonitrile derivatives in the presence of the LDH@PTRMS@DCMBA@CuI nano catalyst is illustrated in Scheme 2. Initially, the interaction of the nano catalyst with the oxygen atom within benzaldehyde initiates the formation of an active electrophilic site, which then initiates an attack on malononitrile. This interaction between reactive aldehydes and malononitrile results in the production of an intermediate

Table 3 Synthesis of 5-amino-1,3-diphenyl-1*H*-pyrazole-4-carbonitrile derivatives in the vicinity of the LDH@PTRMS@DCMBA@CuI catalyst

Time in min, Yield in %, M.p (°C)/ M.p (°C)[Lit.] references

4a, 25 min, 90%
159-161/ 160-162 [33]

4b, 15 min, 93%
128-130/ 128-130 [33]

4c, 17 min, 92%
128-130/127-129 [29]

4d, 16 min, 92%
163-164/ 164-166 [29]

4e, 26 min, 86%
107-109/ 107-108 [29]

4f, 16 min, 93%
161-163/ 162-164 [33]

4g, 23 min, 88%
160-161/ 161-162 [40]

4h, 27 min, 85%
206-208/ 209-211 [29]

4i, 19 min, 89%
163-165/ 145-146 [41]

4j, 24 min, 88%
116-118/ 117-118 [42]

4k, 27 min, 89%
225-227/ new

known as arylidene malononitrile (A).[12] Phenyl hydrazine interacts with intermediate A in the presence of the catalyst, forming intermediate B.[12,42] Next, in the catalyst's vicinity, intermediate B undergoes an intramolecular attack to yield intermediate C.[43] Through tautomerization, intermediate C is converted into intermediate D. Subsequently, intermediate B
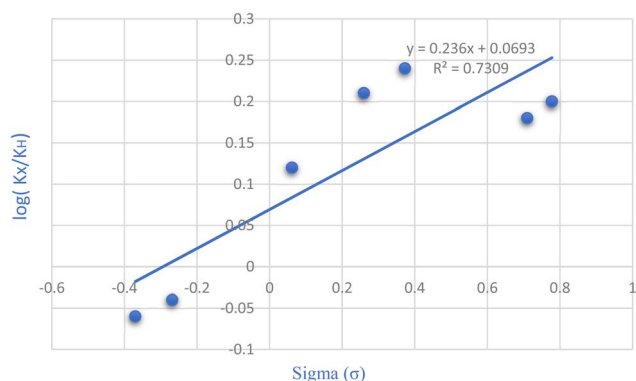
Fig. 8 Investigating the substitution groups in 5-amino-1,3-diphenyl-1*H*-pyrazole-4-carbonitrile synthesis through the Hammett plot.

transforms into intermediate C. This transformation is driven by the anomeric effect, and the electron transfer leads to the formation of intermediate E,[30] where the depicted electrons are transferred into the vacant orbital of the carbon atom. During this step, in the presence of the LDH@PTRMS@DCMBA@CuI catalyst, a negatively charged hydrogen from intermediate D

reacts with a positively charged hydrogen from intermediate E, resulting in the formation and release of a hydrogen molecule, then, the product is synthesized, and the catalyst is recovered for reuse.

The recovery and reusability assessment of the LDH@PTRMS@DCMBA@CuI nanoparticles were conducted under optimal reaction conditions, involving malononitrile (1 mmol), phenyl hydrazine (1 mmol), and 4-chlorobenzaldehyde (1 mmol) in a water/ethanol solvent at 55 °C, utilizing 0.05 g of catalyst. After each cycle, chloroform was introduced into the reaction vessel and stirred for 1 min. Subsequently, the catalyst was isolated from the reaction mixture using centrifugal separation. After the solvent was evaporated, the catalyst was subjected to successive rinses with ethanol before being dried in an oven at 60 °C, ready to be reused in the next cycle. As demonstrated in Fig. 9, the catalyst maintained nearly consistent performance over four consecutive cycles, indicating its robust stability and effectiveness. The graph clearly illustrates that the duration of each recycling reaction period remained relatively unchanged, underscoring the catalyst's ability to sustain its activity without noticeable degradation. The results further confirmed that the catalytic efficiency was not significantly
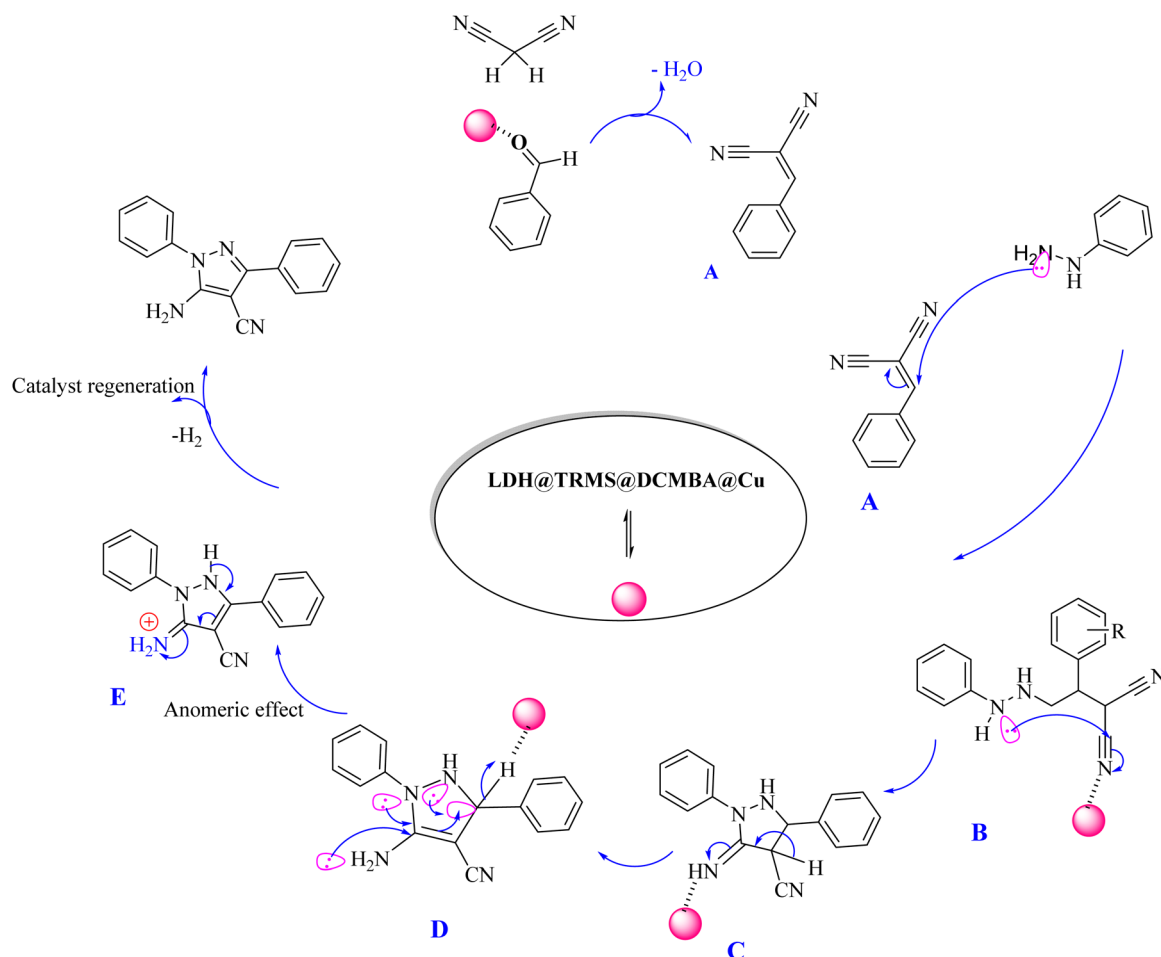
Scheme 2 The proposed mechanism for the synthesis of 5-amino-1,3-diphenyl-1*H*-pyrazole-4-carbonitrile derivatives in the vicinity of the LDH@PTRMS@DCMBA@CuI catalyst.
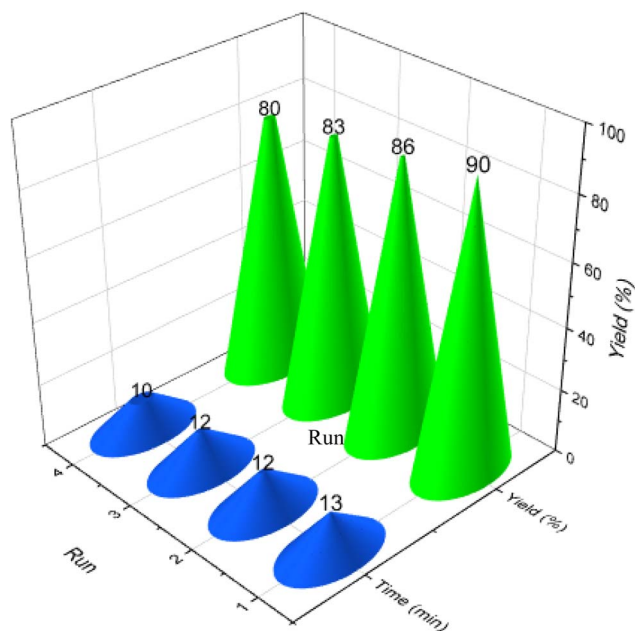
Fig. 9 Ability to recycle and reuse the LDH@PTRMS@DCMBA@CuI catalyst.

diminished across these cycles, showcasing its durability and reliability in repeated use.

The recyclability of the catalyst not only enhances its economic value but also contributes to its environmental sustainability. Each time the catalyst is reused, it undergoes a few simple washes before being deployed in the next cycle, thereby reducing the need for a fresh catalytic material and minimizing waste generation. This repeated use of the catalyst aligns with principles of green chemistry, and reducing the overall environmental impact of the process. The ability to maintain catalytic activity across multiple cycles highlights the potential for long-term application, making this catalyst a valuable asset in both industrial and research settings.

The comparison presented in Table 4 highlights the effectiveness of the LDH@PTRMS@DCMBA@CuI catalytic protocol relative to other catalysts in the synthesis of 5-amino-1,3-diphenyl-1H-pyrazole-4-carbonitrile. Specifically, it demonstrates how this novel catalyst outperforms previous catalysts in

several key metrics, including reaction time, temperature, and yield. The LDH@PTRMS@DCMBA@CuI catalyst achieves higher yield under milder conditions, which significantly enhances the efficiency of the synthesis process. This comparison underscores the superior performance of the LDH@PTRMS@DCMBA@CuI catalyst, making it a more viable and environmentally friendly option for synthesizing pyrazole derivatives.

The LDH@PTRMS@DCMBA@CuI nano catalyst has shown considerable promise for the synthesis of 5-amino-1H-pyrazole-5-carbonitriles, and its potential applications and future research directions are both broad and impactful. Here are several potential avenues that could inspire further studies and demonstrate the ongoing relevance of this work: the catalytic system of LDH@PTRMS@DCMBA@CuI could be extended to the synthesis of other heterocyclic compounds beyond 5-amino-1H-pyrazole-5-carbonitriles. Given the versatility of the catalyst, it could potentially be applied to the formation of other nitrogen-containing heterocycles. Given the biological significance of pyrazole derivatives, future research could explore the use of this catalyst in the synthesis of bioactive compounds, potentially leading to new pharmaceuticals. The development of derivatives with improved biological activity could open up new avenues for drug discovery. By exploring these avenues, researchers can continue to push the boundaries of catalysis and synthetic chemistry, contributing to advancements in various fields.

Future research could focus on kinetic studies and theoretical modeling to uncover the catalyst's role at each step of the reaction. This knowledge could guide the design of more efficient catalysts for similar reactions. Computational chemistry could be employed to design next-generation catalysts based on the LDH@PTRMS@DCMBA@CuI framework. Simulations could help predict the behavior of modified catalysts, identify new ligand systems to achieve even better performance.

4. Conclusion

In summary, a novel LDH@PTRMS@DCMBA@CuI nano catalyst was developed by incorporating copper iodide species onto a nanocomposite derived from layered double hydroxides modified with N_1,N_3-dicarbamimidoylbenzene-1,3-disulfonamide ligand. This catalyst was meticulously validated

Table 4 Comparing the efficiency of the LDH@PTRMS@DCMBA@CuI catalyst in the synthesis of 5-amino-1,3-diphenyl-1H-pyrazole-4-carbonitrile derivatives with some other catalysts

Entry	Reaction conditions	Time (min)	Yield (%)	Lit.
1	Fe_3O_4@CQDs@Si(CH_2)$_3$$NH_2$@CC@EDA@$SO_3H^+Cl^-$, S. F, 89.69 °C	8	83	44
2	[4CSPy]$ZnCl_3$, solvent-free, 80 °C	120	90	41
3	$AlCl_3$, EtOH H_2O, 80 °C	30	83	45
4	Sulfonic acid-functionalized polyvinyl alcohol (SPVA), solvent-free, 90 °C	90	68	40
5	K_2CO_3/glycerol (1 : 4), 80 °C	15	90	46
6	CuO/ZrO_2, H_2O, 40 °C	90	89	47
7	Fe_3O_4@CQD@Si(OEt)(CH_2)$_3$NH@CC@Ad@Cu(OAc)$_2$, S. F, 30 °C	8	54	48
8	Fe_3O_4@Alg@CPTMS@Arg EtOH, reflux	9	86	33
9	MATY-Pd, H_2O, 80 °C, ultrasonic irradiation	25	93	49
10	LDH@PTRMS@DCMBA@Cu, EtOH/H_2O (1 : 1), 55 °C	15	93	This work

using various instrumental techniques, including FTIR, XRD, TGA, DSC, EDX, and mapping analysis. Its efficiency was demonstrated in a one-pot, three-component reaction for synthesizing pyrazole-4-carbonitrile compounds under green conditions. Notably, this method aligns with green chemistry principles by eliminating toxic organic solvents and enabling catalyst recovery. Key advantages of this approach include the use of readily available raw materials, a straightforward one-step reaction process, reduced reaction time, high yield of the product, simple product purification, environmental compatibility, and enhanced yield. Additionally, the catalyst shows exceptional reusability, maintaining remarkable efficiency for up to four cycles and allowing for easy extraction from the reaction mixture.

Data availability

Data is provided within the manuscript or ESI.†

Conflicts of interest

There are no conflicts to declare.

Acknowledgements

References

1 K. Wang, T. Wang, Q. A. Islam and Y. Wu, *Chin. J. Catal.*, 2021, **42**, 1944–1975.

2 Q. Qin, Y. Hu, J. Wang, Y. Yang, T. Lei, Z. Cui, S. Guo and S. Qin, *Nanoscale Adv.*, 2023, **5**, 2873–2878.

3 H. Tian, K. Zhu, Y. Jiang, L. Wang, W. Li, Z. Yu and C. Wu, *Nanoscale Adv.*, 2021, **3**, 2924–2933.

4 E. E. Abdel-Hady, H. F. M. Mohamed, S. H. M. Hafez, A. M. M. Fahmy, A. Magdy, A. S. Mohamed, E. O. Ali, H. R. Abdelhamed and O. M. Mahmoud, *Sci. Rep.*, 2023, **13**, 1–19.

5 S. Momeni and R. Ghorbani-Vaghei, *RSC Adv.*, 2024, **14**, 21608–21622.

6 N. Manna, N. Ayasha, S. K. Singh and S. Kurungot, *Nanoscale Adv.*, 2020, **2**, 1709–1717.

7 X. Zhao, H. Jiang, Y. Xiao and M. Zhong, *Nanoscale Adv.*, 2024, **6**, 1241–1245.

8 W. J. Yan, C. J. Ding, J. J. Min, S. C. Liu, J. Jian, J. Hu and S. Xu, *ACS Sustain. Chem. Eng.*, 2023, **11**, 5216–5228.

9 S. Momeni and R. Ghorbani-Vaghei, *Sci. Rep.*, 2023, **13**, 1–17.

10 S. Kohli, N. Nisha, G. Rathee, S. Hooda and R. Chandra, *Nanoscale Adv.*, 2023, **5**, 2352–2360.

11 S. Teli, S. Soni, P. Teli, N. Sahiba and S. Agarwal, *Res. Chem. Intermed.*, 2024, **50**, 1475–1495.

12 A. Hasaninejad and S. Firoozi, *Mol. Diversity*, 2013, **17**, 459–469.

13 J. Rakhtshah, S. Salehzadeh, E. Gowdini, F. Maleki, S. Baghery and M. A. Zolfigol, *RSC Adv.*, 2016, **6**, 104875–104885.

14 A. Mirzaie, L. Shiri, M. Kazemi, N. Sadeghifard and V. H. Kaviar, *Nanoscale Adv.*, 2024, **6**, 1227–1240.

15 S. Soni, P. Teli, N. Sahiba, S. Teli and S. Agarwal, *RSC Adv.*, 2023, **13**, 13337–13353.

16 S. Sangwan, R. Singh, S. Gulati and S. Rana, *Curr. Res. Green Sustainable Chem.*, 2021, **4**, 100146.

17 S. B. Katiyar, K. Srivastava, S. K. Puri and P. M. S. Chauhan, *Bioorg. Med. Chem. Lett.*, 2005, **15**, 4957–4960.

18 A. Bekhit and T. Abdel-Aziem, *Bioorg. Med. Chem.*, 2004, **12**, 1935–1945.

19 P. Teli, N. Sahiba, A. Manhas, P. C. Jha, P. Meena and S. Agarwal, *ChemistrySelect*, 2023, **8**, e202204806.

20 A. Bernardino, A. Gomes, A. Gomes, K. Charret, A. Freitas, G. Machado, M. Canto-Cavalheiro and V. Amaral, *Eur. J. Med. Chem.*, 2006, **41**, 80–87.

21 S. H. Allen, B. A. Johns, K. S. Gudmundsson, G. A. Freeman, F. L. Boyd, C. H. Sexton, D. W. Selleseth, K. L. Creech and K. R. Moniri, *Bioorg. Med. Chem.*, 2006, **14**, 944–954.

22 D. M. Bailey, P. E. Hansen, A. G. Hlavac, E. R. Baizman, J. Pearl, A. F. DeFelice and M. E. Feigenson, *J. Med. Chem.*, 1985, **28**, 256–260.

23 I. El-Deeb and S. Lee, *Bioorg. Med. Chem.*, 2010, **18**, 3961–3973.

24 A. Tewari and A. Mishra, *Bioorg. Med. Chem.*, 2001, **9**, 715–718.

25 T. D. Penning, J. J. Talley, S. R. Bertenshaw, J. S. Carter, P. W. Collins, S. Docter, M. J. Graneto, L. F. Lee, J. W. Malecha, J. M. Miyashiro, R. S. Rogers, D. J. Rogier, S. S. Yu, G. D. Anderson, E. G. Burton, J. N. Cogburn, S. A. Gregory, C. M. Koboldt, W. E. Perkins, K. Seibert, A. W. Veenhuizen, Y. Y. Zhang and P. C. Isakson, *J. Med. Chem.*, 1997, **40**, 1347–1365.

26 N. K. Terrett, A. S. Bell, D. Brown and P. Ellis, *Bioorg. Med. Chem. Lett.*, 1996, **6**, 1819–1824.

27 N. Yadav, R. Singh and Y. K. Tyagi, *Org. Prep. Proced. Int.*, 2024, 1–8.

28 M. J. Genin, C. Biles, B. J. Keiser, S. M. Poppe, S. M. Swaney, W. G. Tarpley, Y. Yagi and D. L. Romero, *J. Med. Chem.*, 2000, **43**, 1034–1040.

29 H. Kiyani and M. Bamdad, *Res. Chem. Intermed.*, 2018, **44**, 2761–2778.

30 M. A. Zolfigol, F. Afsharnadery, S. Baghery, S. Salehzadeh and F. Maleki, *RSC Adv.*, 2015, **5**, 75555–75568.

31 N. Singh and J. Pandey, *Curr. Res. Green Sustainable Chem.*, 2021, **4**, 100134.

32 P. Arora and J. K. Rajput, *J. Mater. Sci.*, 2017, **52**, 11413–11427.

33 S. Amirnejat, A. Nosrati and S. Javanshir, *Appl. Organomet. Chem.*, 2020, **34**, 1–13.

34 C. Ma, P. Wen, J. Li, X. Han, Z. Wu and G. Huang, *Adv. Synth. Catal.*, 2016, **358**, 1073–1077.

35 M. Srivastava, P. Rai, J. Singh and J. Singh, *RSC Adv.*, 2013, **3**, 16994–16998.

36 N. Esfandiary, A. Nakisa, K. Azizi, J. Azarnia, I. Radfar and A. Heydari, *Appl. Organomet. Chem.*, 2017, **31**, e3641.

37 S. Momeni and R. Ghorbani-Vaghei, *ACS Omega*, 2024, **9**, 10332–10342.

38 S. Momeni and R. Ghorbani-Vaghei, *Sci. Rep.*, 2023, **13**, 1627.

39 S. Momeni and R. Ghorbani-Vaghei, *J. Mol. Struct.*, 2023, **1288**, 135758.

40 A. S. Patki, K. N. Patil, S. Kusuma, D. B. Muley and A. H. Jadhav, *Res. Chem. Intermed.*, 2021, **47**, 2751–2773.

41 A. R. Moosavi-Zare, M. Rezaei-Gohar, M. Tavasoli and H. Goudarziafshar, *Res. Chem. Intermed.*, 2021, **47**, 2689–2700.

42 A. S. Patki, K. N. Patil, S. Kusuma, D. B. Muley and A. H. Jadhav, *Res. Chem. Intermed.*, 2021, **47**, 2751–2773.

43 S. Poonam and R. Singh, *Res. Chem. Intermed.*, 2019, **45**, 4531–4542.

44 N. Sarmasti, J. Yousefi Seyf and A. Khazaei, *Arabian J. Chem.*, 2021, **14**, 103026.

45 D. Mishra, R. Singh and C. Rout, *J. Chem. Pharm. Res.*, 2017, **9**, 16–19.

46 A. A. Zwain, I. Ahmad, R. Khalaf Jebur Ali, M. Kahtan, A. Khdyair Hamad, E. Abdulgader Hassan, M. Asiri, B. M. Ridha and A. Alsalamy, *Front. Mater.*, 2023, **10**, 1–10.

47 S. Maddila, S. Rana, R. Pagadala, S. Kankala, S. Maddila and S. B. Jonnalagadda, *Catal. Commun.*, 2015, **61**, 26–30.

48 A. Gorji, T. Akbarpour and A. Khazaei, *Polycyclic Aromat. Compd.*, 2023, **43**, 5041–5073.

49 M. A. E. A. A. Ali El-Remaily, T. El-Dabea, M. Alsawat, M. H. H. Mahmoud, A. A. Alfi, N. El-Metwaly and A. M. Abu-Dief, *ACS Omega*, 2021, **6**, 21071–21086.

© 2024 The Author(s). Published by the Royal Society of Chemistry